Triple Regge exchange mechanisms of four-pion continuum production in the $pp \to pp\pi^+\pi^-\pi^+\pi^-$ reaction

Radosław Kycia,[1,*] Piotr Lebiedowicz,[2,†] Antoni Szczurek,[2,‡] and Jacek Turnau[3,§]

[1]*Cracow University of Technology, Faculty of Physics, Mathematics and Computer Science, PL-31155 Kraków, Poland*

[2]*Institute of Nuclear Physics Polish Academy of Sciences, PL-31342 Kraków, Poland*

[3]*Hetmańska 5, Kraków, PL-30528, Poland*

(Received 27 March 2017; published 26 May 2017)

We consider exclusive multiperipheral production of four charged pions in proton-proton collisions at high energies with simultaneous exchange of three Pomerons/Reggeons. The amplitude(s) for the genuine $2 \to 6$ process are written in the Regge approach. The calculation is performed with the help of the GenEx Monte Carlo code. Some corrections at low invariant masses in the two-body subsystems are necessary for application of the Regge formalism. We estimate the corresponding cross section and present differential distributions in rapidity, transverse momenta and two- and four-pion invariant masses. The cross section and the distributions depend on the value of the cutoff parameter of a form factor correcting amplitudes for off-shellness of t-channel pions. A rather large cross section is found for the whole phase space ($\sigma \sim 1$–5 μb, including absorption corrections). Relatively large four-pion invariant masses are populated in the considered diffractive mechanism compared to other mechanisms discussed so far in the context of four-pion production. We investigate whether the triple Regge exchange processes could be identified with the existing LHC detectors. We consider the case of ATLAS and ALICE cuts. The ATLAS (or CMS) has a better chance to identify the process in the region of large invariant masses $M_{4\pi} > 10$ GeV. In the case of the ALICE experiment the considered mechanism competes with other mechanisms (production of $\sigma\sigma$, $\rho\rho$ pairs or single resonances) and cannot be unambiguously identified.

DOI: 10.1103/PhysRevD.95.094020

I. INTRODUCTION

In the present paper, we study the exclusive $2 \to 6$ process,

$$pp \to pp\pi^+\pi^-\pi^+\pi^-. \tag{1.1}$$

In general, the number of possible mechanisms is rather large. Here we shall focus on the triple Regge exchange processes. According to our knowledge such processes have not been discussed quantitatively in the literature, and estimation of their importance becomes timely in the light of studies being performed by the STAR, ATLAS, CMS and ALICE collaborations. At the LHC the energy is so high that there is enough rapidity span for such processes to occur, at least from the theoretical point of view.

In this study we present an extension of the Regge-inspired Lebiedowicz-Szczurek approach used for the reactions $pp \to pp\pi^+\pi^-$ [1,2], $pp \to nn\pi^+\pi^+$ [3] and $pp \to ppK^+K^-$ [4]. The number of diagrams for the six-body reactions is bigger than for the four-body reaction and we have to carefully write the corresponding amplitudes using simplified Regge rules for πp and $\pi\pi$ interactions.

We shall try to use the same model parameters as for the $pp \to pp\pi^+\pi^-$ process whenever possible. This should allow for an approximate estimation of the cross section and some differential distributions. The calculation presented here is performed with the help of the GenEx Monte Carlo event generator [5].

We wish to concentrate on the four-charged-pion continuum production mechanism which, in addition, is a background for studies of central exclusive production of resonances discussed recently in [6]. The production of glueball states is expected to be enhanced in gluon-rich Pomeron-Pomeron interactions. Identification of diffractively produced glueball states is still an experimental challenge at the LHC. For the experimental point of view at lower energies see e.g. [7]. This requires calculation or estimation of the four-pion background from different sources, see e.g. [8].

II. AMPLITUDE FOR THE FOUR-PION CONTINUUM PRODUCTION

The general situation for the $pp \to pp\pi^+\pi^-\pi^+\pi^-$ process is sketched in Fig. 1. The full amplitude,

*Also at Faculty of Science, Masaryk University, Kotlářská 2, 602 00 Brno, Czech Republic.
kycia.radoslaw@gmail.com
†Piotr.Lebiedowicz@ifj.edu.pl
‡Also at the Faculty of Mathematics and Natural Sciences, University of Rzeszow, ul. Pigonia 1, 35-310 Rzeszow, Poland.
Antoni.Szczurek@ifj.edu.pl
§turnauster@gmail.com

 © 2017 American Physical Society

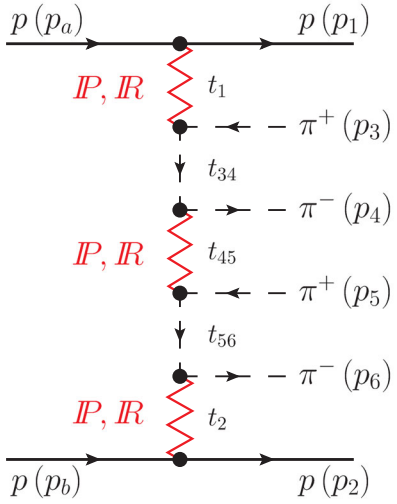

FIG. 1. A diagram for exclusive diffractive production of $\pi^+\pi^-\pi^+\pi^-$ continuum with three Pomeron/Reggeon exchanges in proton-proton collisions. Here $\mathbb{R}$ denotes the $f_{2\mathbb{R}}$ or $\rho_{\mathbb{R}}$ Reggeon exchanges. The four-momentum transfers squared are shown explicitly.

including different permutations of outgoing pion pairs, can be written as[1]

$$\begin{aligned}\mathcal{M} = &\frac{1}{2}(\mathcal{M}_{\{3456\}} + \mathcal{M}_{\{5436\}} + \mathcal{M}_{\{3654\}} + \mathcal{M}_{\{5634\}}) \\ &+ \frac{1}{2}(\mathcal{M}_{\{4356\}} + \mathcal{M}_{\{4536\}} + \mathcal{M}_{\{6354\}} + \mathcal{M}_{\{6534\}}) \\ &+ \frac{1}{2}(\mathcal{M}_{\{3465\}} + \mathcal{M}_{\{5463\}} + \mathcal{M}_{\{3645\}} + \mathcal{M}_{\{5643\}}) \\ &+ \frac{1}{2}(\mathcal{M}_{\{4365\}} + \mathcal{M}_{\{4563\}} + \mathcal{M}_{\{6345\}} + \mathcal{M}_{\{6543\}}),\end{aligned} \tag{2.1}$$

where the factor $\frac{1}{2}$ is the symmetry factor for two identical pions.[2]

In the formulas below the subsystem energies squared is

$$s_{ij} = M_{ij}^2 = (p_i + p_j)^2, \tag{2.2}$$

where p_i and p_j are respective four-vectors, and the formulas of four-momentum transfers squared are[3]

$$\begin{aligned}t_1 &= (p_a - p_1)^2, \\ t_2 &= (p_b - p_2)^2, \\ t_{34} &= (p_a - p_1 - p_3)^2, \\ t_{43} &= (p_a - p_1 - p_4)^2, \\ t_{45} &= t_{35} = t_{46} = t_{36} = (p_a - p_1 - p_3 - p_4)^2 \\ &= (p_b - p_2 - p_6 - p_5)^2, \\ t_{56} &= (p_b - p_2 - p_6)^2, \\ t_{65} &= (p_b - p_2 - p_5)^2.\end{aligned} \tag{2.3}$$

We write the amplitude for each group in Eq. (2.1),

$$\begin{aligned}\mathcal{M}_{\{3456\}} = &A_{\pi p}(s_{13}, t_1)\frac{F_\pi(t_{34})}{t_{34} - m_\pi^2}A_{\pi\pi}(s_{45}, t_{45}) \\ &\times \frac{F_\pi(t_{56})}{t_{56} - m_\pi^2}A_{\pi p}(s_{26}, t_2),\end{aligned} \tag{2.4}$$

$$\begin{aligned}\mathcal{M}_{\{4356\}} = &A_{\pi p}(s_{14}, t_1)\frac{F_\pi(t_{43})}{t_{43} - m_\pi^2}A_{\pi\pi}(s_{35}, t_{35}) \\ &\times \frac{F_\pi(t_{56})}{t_{56} - m_\pi^2}A_{\pi p}(s_{26}, t_2),\end{aligned} \tag{2.5}$$

$$\begin{aligned}\mathcal{M}_{\{3465\}} = &A_{\pi p}(s_{13}, t_1)\frac{F_\pi(t_{34})}{t_{34} - m_\pi^2}A_{\pi\pi}(s_{46}, t_{46}) \\ &\times \frac{F_\pi(t_{65})}{t_{65} - m_\pi^2}A_{\pi p}(s_{25}, t_2),\end{aligned} \tag{2.6}$$

$$\begin{aligned}\mathcal{M}_{\{4365\}} = &A_{\pi p}(s_{14}, t_1)\frac{F_\pi(t_{43})}{t_{43} - m_\pi^2}A_{\pi\pi}(s_{36}, t_{36}) \\ &\times \frac{F_\pi(t_{65})}{t_{65} - m_\pi^2}A_{\pi p}(s_{25}, t_2).\end{aligned} \tag{2.7}$$

The subprocess amplitudes with the Regge exchanges are given as

$$A_{\pi p}(s,t) = \sum_{j=\mathbb{P}, f_{2\mathbb{R}}} \eta_j s C_{\pi p}^j \left(\frac{s}{s_0}\right)^{\alpha_j(t)-1} F_{\pi p}^j(t), \tag{2.8}$$

$$A_{\pi\pi}(s,t) = \sum_{j=\mathbb{P}, f_{2\mathbb{R}}} \eta_j s C_{\pi\pi}^j \left(\frac{s}{s_0}\right)^{\alpha_j(t)-1} F_{\pi\pi}^j(t), \tag{2.9}$$

where the signature factors at $t = 0$ are $\eta_{\mathbb{P}} = i$ and $\eta_{f_{2\mathbb{R}}} = i - 0.86$ [1]. The interaction strength parameters are assumed to fulfill the Regge factorization relation

$$C_{pp}^j C_{\pi\pi}^j = C_{\pi p}^j C_{\pi p}^j, \tag{2.10}$$

where $j = \mathbb{P}, f_{2\mathbb{R}}$. In our calculations we use the following numerical parameters:

[1]Here we introduce a shorthand notation that corresponds to the four-momenta of outgoing pions; e.g. $\{3456\}$ means that the index 3 is for $\pi^+(p_3)$, index 4 is for $\pi^-(p_4)$, index 5 is for another $\pi^+(p_5)$, and index 6 is for another $\pi^-(p_6)$, see the diagram in Fig. 1.

[2]The symmetry factor is artificially written here instead of the factor $\frac{1}{2!2!}$ in the cross-section formula.

[3]Here p_1, p_2, p_3, p_4, p_5, p_6 should be treated as outgoing.

$$C^{\mathbb{P}}_{pp} = 21.70\,\text{mb}, \quad C^{\mathbb{P}}_{\pi p} = 13.63\,\text{mb}, \quad C^{\mathbb{P}}_{\pi\pi} = 8.56\,\text{mb}, \tag{2.11}$$

$$C^{f_{2\mathbb{R}}}_{pp} = 75.4875\,\text{mb}, \quad C^{f_{2\mathbb{R}}}_{\pi p} = 31.79\,\text{mb}, \quad C^{f_{2\mathbb{R}}}_{\pi\pi} = 13.39\,\text{mb}. \tag{2.12}$$

We parametrize the t-dependences of subprocess amplitudes in the exponential form

$$F^j_{\pi p}(t) = \exp\left(\frac{B^j_{\pi p}}{2}t\right), \tag{2.13}$$

$$F^j_{\pi\pi}(t) = \exp\left(\frac{B^j_{\pi\pi}}{2}t\right), \tag{2.14}$$

where the slope parameters are taken as $B^{\mathbb{P}}_{\pi p} = 5.5\ \text{GeV}^{-2}$, $B^{\mathbb{P}}_{\pi\pi} = 4\ \text{GeV}^{-2}$, $B^{f_{2\mathbb{R}}}_{\pi p} = 4\ \text{GeV}^{-2}$ and $B^{f_{2\mathbb{R}}}_{\pi\pi} = 4\ \text{GeV}^{-2}$ (see [1]).

The small-t dependence, see Eqs. (2.8), (2.9) and (2.13), (2.14), is known to deviate from purely exponential dependence. This was discussed in the context of elastic scattering in [9] but also for the $pp \to pp\pi^+\pi^-$ reaction in [6]. We leave this point for our $pp \to pp\pi^+\pi^-\pi^+\pi^-$ process for future studies. Explicit inclusion of absorption would dynamically generate deviations from exponential form but this goes far beyond the scope of our present paper.

The Regge trajectories $\alpha_j(t)$ are assumed to be of the standard linear form [10],

$$\alpha_j(t) = \alpha_j(0) + \alpha'_j t, \tag{2.15}$$

$$\alpha_{\mathbb{P}}(0) = 1.0808, \qquad \alpha'_{\mathbb{P}} = 0.25\ \text{GeV}^{-2}, \tag{2.16}$$

$$\alpha_{f_{2\mathbb{R}}}(0) = 0.5475, \qquad \alpha'_{f_{2\mathbb{R}}} = 0.9\ \text{GeV}^{-2}. \tag{2.17}$$

Above, f_{2R} means a f_2 Reggeon. The parameters of f_{2R} in Eq. (2.17) were extracted from [1] based on Donnachie-Landshoff fits [10] but must be considered as effective.

The off-shellness of t-channel pions in the diagrams is included via multiplication of corresponding amplitudes by the extra form factor,

$$F_\pi(t) = \exp\left(\frac{t - m_\pi^2}{\Lambda^2_{\text{off},E}}\right) = \exp\left(\frac{t - m_\pi^2}{2\Lambda^2_{\text{off},E}}\right)\exp\left(\frac{t - m_\pi^2}{2\Lambda^2_{\text{off},E}}\right). \tag{2.18}$$

In fact the off-shell effects are related to vertices and they always go in pairs for our process. The form factor is normalized to unity when meson is on-mass-shell $F_\pi(m_\pi^2) = 1$. The parameter of the off-shell form factor is in principle a free parameter. In the present paper we shall use $\Lambda_{\text{off},E} = 1$ GeV (lower limit) and use $\Lambda_{\text{off},E} = 1.5$ GeV (upper limit). These values correspond to $\tilde{\Lambda}_{\text{off},E} = 1.41$ GeV and $\tilde{\Lambda}_{\text{off},E} = 2.12$ GeV in the convention used in [1].

The amplitudes (2.8) and (2.9) have to be corrected for low $\sqrt{s_{ij}} = W_{ij}$ as the Regge theory is valid only above a lower subenergy limit. In our analysis here mainly a smooth cutoff function will be used, as in [1], e.g.,

$$f_{\text{cont}}(W_{ij}) = \frac{\exp\left((W_{ij} - W_0)/a\right)}{1 + \exp\left((W_{ij} - W_0)/a\right)}, \tag{2.19}$$

with $a = 0.2$ GeV and $W_0 = 2$ GeV, which cuts off $s_{ij} \lesssim 4\ \text{GeV}^2$ smoothly.

Another cutoff function which we use is the Heaviside theta function,

$$f_{\text{discont}}(W_{ij}) = \theta(W_{ij} - W_{\text{cut}}), \tag{2.20}$$

where W_{cut} is a parameter to be adjusted to future precise data. We will show that both functions, see (2.19) and (2.19), give similar results for the integrated cross section; however, they give somewhat different distributions in some special variables.

III. FEASIBILITY STUDY FOR THE MEASUREMENT OF THE TRIPLE REGGE EXCHANGE PROCESS AT CURRENT LHC EXPERIMENTS

In this section we show some predictions for the considered process. We will select $\sqrt{s} = 7$ TeV collision energy as a representative example. The collision energy dependence of the cross section is rather weak (see Sec. IV E).

Presentation of our results is divided into three parts:

(A) calculation for the full six-body phase space,
(B) calculation relevant for the ATLAS main tracker,
(C) calculation relevant for the ALICE main tracker.

In a separate section we discuss some general specific aspects of the mechanism discussed here.

Some technical details related to the Monte Carlo integration are described in the Appendix.

A. Results for the full phase space

In this subsection we present some results for cross-section calculation which we call "full phase space," meaning that only minimal cuts are imposed for purely technical reasons, namely

$$p_{t,p} < 2\,\text{GeV}, \quad |y_{4\pi}| < 6, \quad M_{4\pi} < 30\,\text{GeV}. \tag{3.1}$$

These cuts can be easily placed in experimental analyses and do not change the shape of the resulting distributions.

TABLE I. Full phase space cross sections in μb. No absorption effects are included here.

	$\Lambda_{\mathrm{off},E}$ (GeV)	σ (μb)
Symmetrization	1.0	7.21
No symmetrization	1.0	0.82
Symmetrization	1.5	42.86
No symmetrization	1.5	4.30

The condition $M_{4\pi} < 30$ GeV cuts off less than a few percent of the cross section.

In Table I we present numerical results for the cross section integrated over the so-defined full phase space. In the table, "No symmetrization" means that we take only one arbitrarily chosen term for the matrix element and omit the symmetrization factor; that is, $\mathcal{M} = \mathcal{M}_{\{3456\}}$ in Eq. (2.4).

In Figs. 2, 3, 4 and 7 the general features of the investigated process are presented while Figs. 5 and 6 illustrate relative contributions of the Pomeron and subleading Reggeon trajectories to the calculated cross sections.

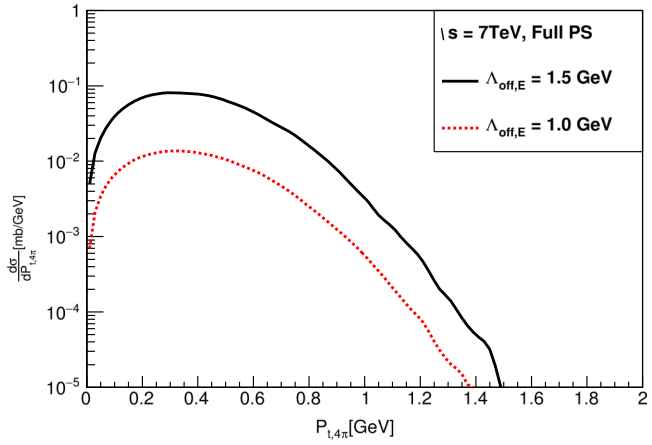

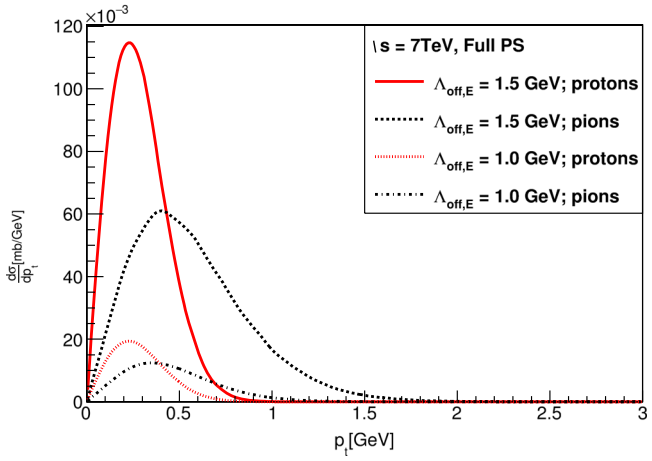

FIG. 2. Distributions in transverse momentum of the four-pion system and for the transverse momenta of individual particles (protons and pions) for two different values of $\Lambda_{\mathrm{off},E} = 1$, 1.5 GeV.

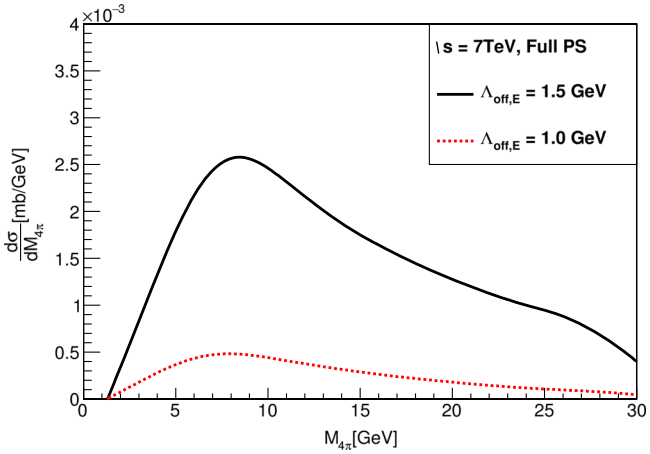

FIG. 3. Four-pion invariant mass distribution for the full phase space for two different values of $\Lambda_{\mathrm{off},E} = 1$, 1.5 GeV.

The distribution in four-pion invariant mass, see Fig. 3, extends in relatively broad range, compared e.g. to dipion invariant mass distribution for the $pp \to pp\pi^+\pi^-$ reaction. The four-momentum transfer from both protons to the 4π system is restricted by the peripherality of the process which results in relatively narrow distribution of (4.2) shown in Fig. 21.

At $\sqrt{s} = 7$ TeV the outgoing protons are produced at $y \approx \pm 9$ (see Fig. 4). The pions are produced between protons. The pion rapidity distribution illustrates well the role of subleading $f_{2\mathbb{R}}$ Reggeons. In Fig. 5 we compare distributions for $(\mathbb{P} + f_{2\mathbb{R}}) \times (\mathbb{P} + f_{2\mathbb{R}}) \times (\mathbb{P} + f_{2\mathbb{R}})$ and $\mathbb{P} \times \mathbb{P} \times \mathbb{P}$ exchanges. Here the notation corresponds to external $\times$ internal $\times$ external exchanges (see Fig. 1). Adding $f_{2\mathbb{R}}$ exchange not only enhances the cross section but also modifies the shape of the distribution. One can

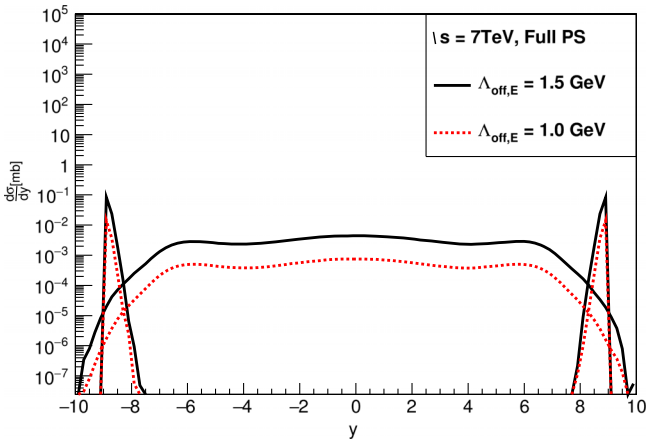

FIG. 4. Rapidity distribution of protons (external peaks) and pions (internal bumps) for the full phase space for two different values of $\Lambda_{\mathrm{off},E} = 1$, 1.5 GeV.

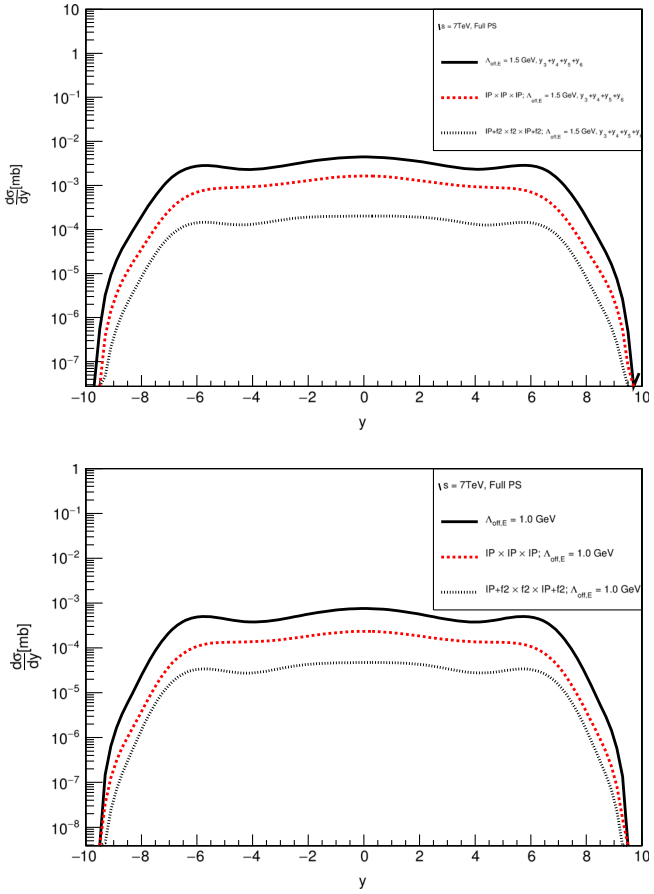

FIG. 5. Rapidity distribution of pions for $(\mathbb{P}+f_{2\mathbb{R}})\times(\mathbb{P}+f_{2\mathbb{R}})\times(\mathbb{P}+f_{2\mathbb{R}})$ (upper curve), $\mathbb{P}\times\mathbb{P}\times\mathbb{P}$ (middle curve) and $(\mathbb{P}+f_{2\mathbb{R}})\times f_{2\mathbb{R}}\times(\mathbb{P}+f_{2\mathbb{R}})$ (lower curve) exchanges for two different values of $\Lambda_{\mathrm{off},E}=1$, 1.5 GeV.

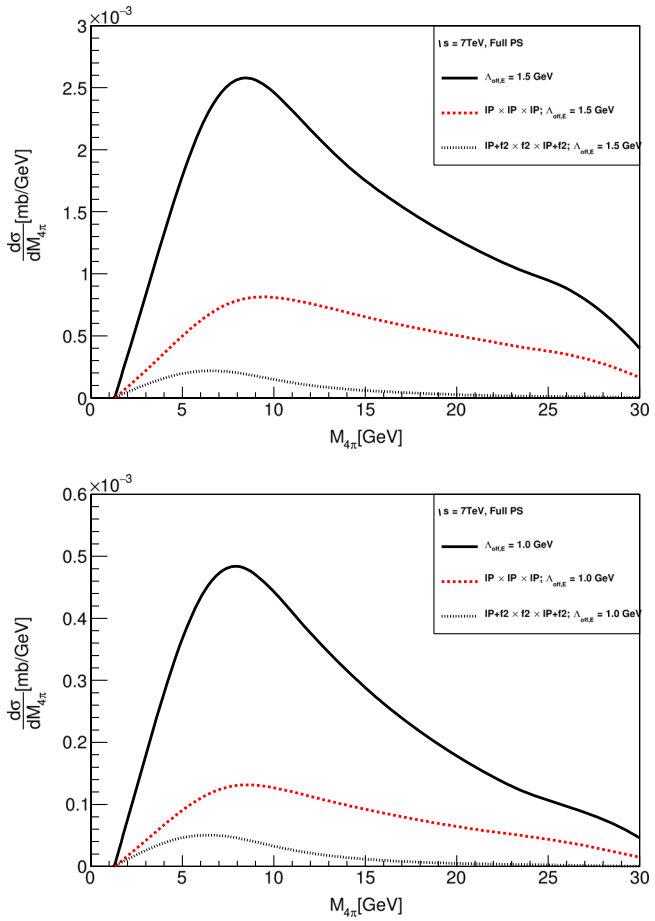

FIG. 6. 4π invariant mass distribution for $(\mathbb{P}+f_{2\mathbb{R}})\times(\mathbb{P}+f_{2\mathbb{R}})\times(\mathbb{P}+f_{2\mathbb{R}})$ (upper curve), $\mathbb{P}\times\mathbb{P}\times\mathbb{P}$ (middle curve) and $(\mathbb{P}+f_{2\mathbb{R}})\times f_{2\mathbb{R}}\times(\mathbb{P}+f_{2\mathbb{R}})$ (lower curve) exchanges for two different values of $\Lambda_{\mathrm{off},E}=1$, 1.5 GeV.

observe now clear enhancements at $y\approx\pm6$ that correspond to the external exchanges of $f_{2\mathbb{R}}$ Reggeons. This figure reminds us of a similar figure for the $pp\to pp\pi^+\pi^-$ reaction, where a camel-like distribution was obtained [1]. There the peaks at large rapidities correspond to $f_{2\mathbb{R}}$ Reggeon exchanges. Here (for the $pp\to pp\pi^+\pi^-\pi^+\pi^-$ reaction) three peaks can be observed. In addition, we plot $(\mathbb{P}+f_{2\mathbb{R}})\times f_{2\mathbb{R}}\times(\mathbb{P}+f_{2\mathbb{R}})$ when in the middle only $f_{2\mathbb{R}}$ is present. The cross section is significantly smaller, which means that $\mathbb{P}$ in the middle of the diagram is responsible for the cross section enhancement. There is a qualitative hydromechanical analogy in which all outgoing particles in diagrams (shown schematically in Fig. 1) are represented as liquid layers which move with parallel velocities and protons are the top and bottom layers. Then the coupling/friction between layers is given by the parameters of the Pomeron/Reggeon exchanges. In Fig. 6, $M_{4\pi}$ distributions for $(\mathbb{P}+f_{2\mathbb{R}})\times(\mathbb{P}+f_{2\mathbb{R}})\times(\mathbb{P}+f_{2\mathbb{R}})$, $\mathbb{P}\times\mathbb{P}\times\mathbb{P}$ and $(\mathbb{P}+f_{2\mathbb{R}})\times f_{2\mathbb{R}}\times(\mathbb{P}+f_{2\mathbb{R}})$ are plotted. We can see that at $\Lambda_{\mathrm{off},E}=1.5$ GeV and $M_{4\pi}\approx8$ GeV the triple Pomeron exchange contributes $\approx1/3$ of the cross section, reaching $\approx1/2$ at 30 GeV. These ratios are even smaller for $\Lambda_{\mathrm{off},E}=1$ GeV.

In Fig. 7 we discuss distribution in dipion invariant mass separately for the opposite-sign pions (left panel) and for the same-sign pions (right panel). To improve statistics and reduce fluctuations, the distributions for different combinations of indices (34, 56, 36, 45 for the opposite-sign pions or 35, 46 for the same-sign pions) were averaged in all figures of this type. The distributions for the opposite-sign pions have a large component at low ($M_{\pi\pi}<3$ GeV) dipion invariant mass, similarly to the dipion mass distribution for the exclusive dipion production (see e.g. [6]). The distribution for the same-sign pions is clearly broader than that for the opposite-sign pions and has a maximum at larger invariant masses. This is due to the possible presence of the rapidity gap between the two $\pi^+\pi^-$ pairs, as illustrated in Figs. 23 and 24, where we plot the differential cross section for the $(+-)(+-)+(-+)(-+)$, $(+-)(-+)+(-+)(-+)$ and $(++)(--)+(--)(++)$ configurations of ordered in rapidity pions as a function

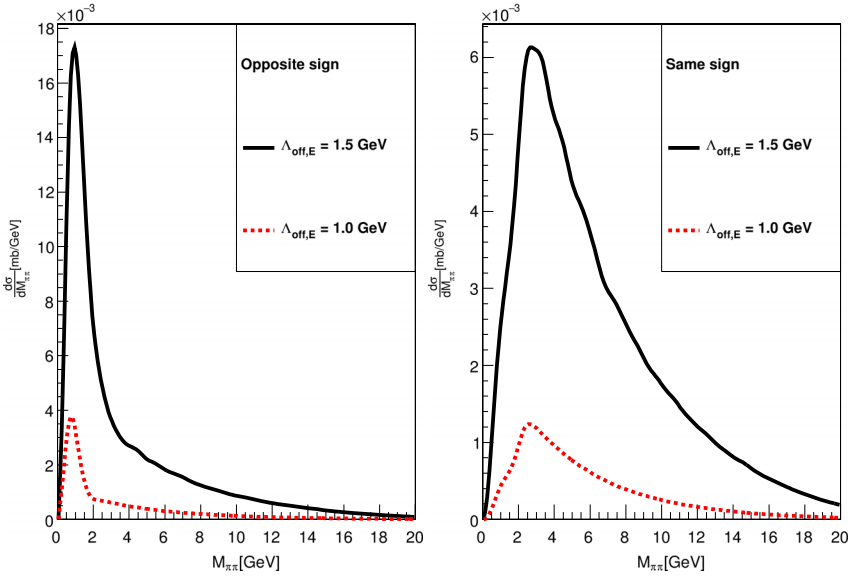

FIG. 7. Dipion invariant mass distributions for the opposite-sign (left) and for the same-sign (right) pions for two different values of $\Lambda_{\mathrm{off},E} = 1$ GeV (lower curve) and $\Lambda_{\mathrm{off},E} = 1.5$ GeV (upper curve).

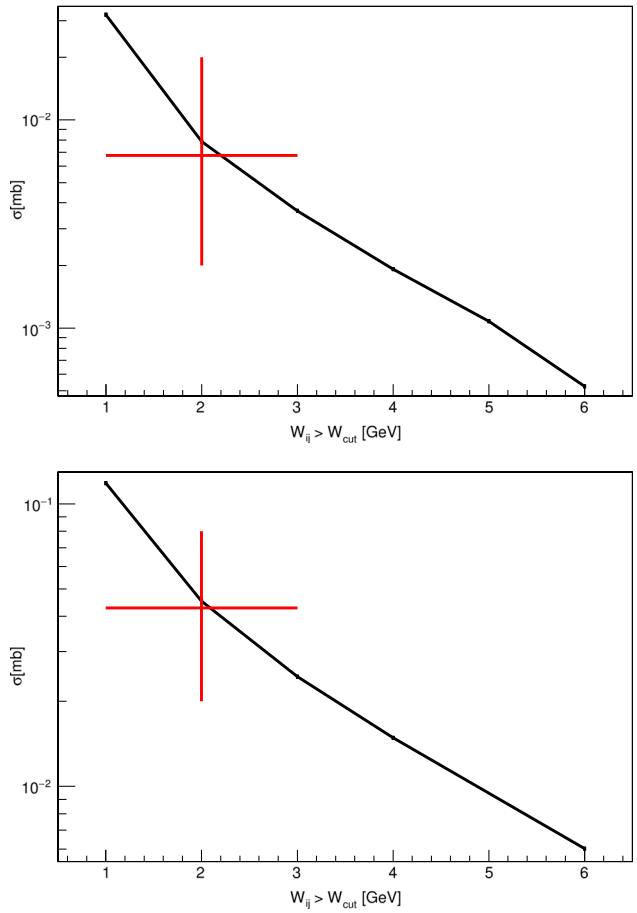

FIG. 8. Integrated cross section for different values of W_{cut} for a sharp (Heaviside-like) cutoff function. The extra (red) cross represents the cross section for the smooth cutoff function with $W_0 = 2$ GeV and $a = 0.2$ GeV as taken from [1]. The upper plot is for $\Lambda_{\mathrm{off},E} = 1$ GeV and the lower one for $\Lambda_{\mathrm{off},E} = 1.5$ GeV.

of the central rapidity gap width. It is clear that the same-sign pion pairs are often formed across the large rapidity gap, what is reflected by the width of their invariant mass distribution, Fig. 7. This is also related to the somewhat arbitrary cutoff approach to the region where the Regge formalism (2.9) does not apply. The higher invariant dipion masses are only weakly dependent on the cutoff of the low masses of the two pions across the Pomeron/Reggeon exchange. It is not clear to us how to correctly include this region.

The shapes of the distributions in dipion invariant masses only slightly depend on the value of the cutoff parameter of the off-shell form factor (2.18). The position of the maximum for the same-sign pions at $M_{\pi\pi} \sim 3$ GeV seems to be related to the point in $M_{\pi\pi}$ where we gradually screen off the Regge amplitude [see Eq. (2.18)]. The position of the transition from the Regge to non-Regge physics have been taken here (somewhat arbitrarily) to be 3 GeV. Therefore our predictions are valid above $M_{\pi\pi} > 3$ GeV. What happens below $M_{\pi\pi} = 3$ GeV is rather a matter of future measurements. Clearly our approach is not valid in this region and therefore has no predictive power there.

For illustration in Fig. 8 we show dependence of the integrated cross section on the sharp cutoff parameter W_{cut} [see Eq. (2.20)]. One can observe a powerlike dependence of the cross section as a function of W_{cut}. The extra crosses in the figure show the value of W_0 and the corresponding cross section in the smooth cutoff approach [see Eq. (2.19)]. Such a value of W_0 was used in the description of the $pp \to pp\pi^+\pi^-$ process (see [1]). As it is seen the cross section for $W_0 = 2$ GeV (smooth cutoff) is very much the same as the cross section for $W_{\mathrm{cut}} \sim 2$–2.5 GeV (sharp cutoff).

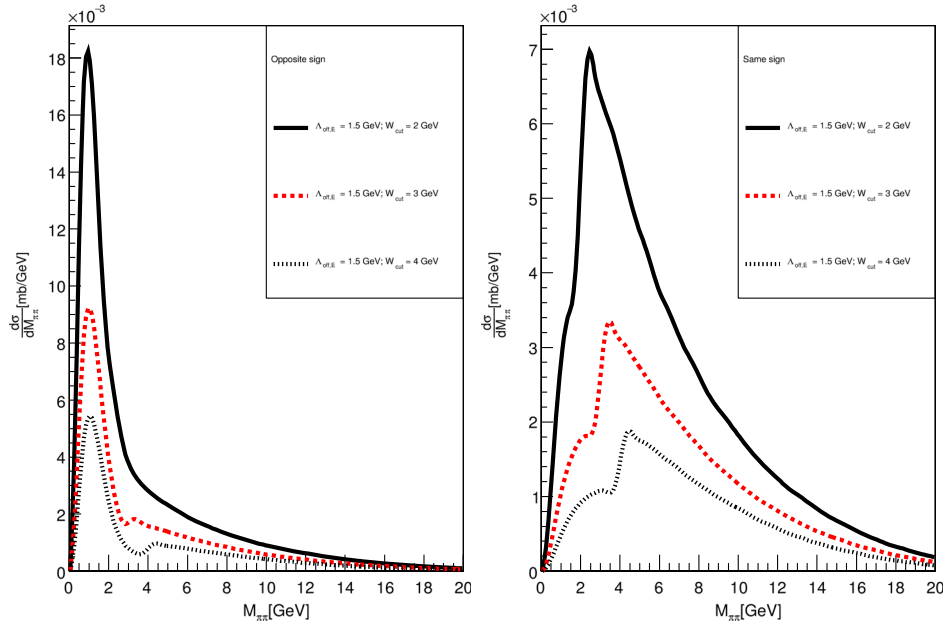

FIG. 9. Dipion invariant mass distributions for the opposite-sign (left) and the same-sign (right) pions for different values of $W_{\rm cut}$ for sharp cutoff function (2.20) and $\Lambda_{{\rm off},E} = 1.5$ GeV.

Finally, in Fig. 9 we show how the choice of $W_{\rm cut}$ (sharp cutoff) influences the distributions. As an example we consider dipion mass spectra, where the effect of the cutoff function is the most visible. In this calculation we fixed $\Lambda_{{\rm off},E} = 1.5$ GeV and we show results for three different values of $W_{\rm cut}$. The sharp cutoff leads to characteristic sudden increase of the cross section. The large part of the dipion distributions is only weakly dependent on the value of $W_{\rm cut}$, but some visible effect survives (see the location of the dips in Fig. 9). This means that the different dipion subsystems are to some extent correlated. The study performed here was only to illustrate the possible uncertainties of our predictions. However, we believe that our default smooth cutoff is the optimal choice at present. We feel one should return to the problem when corresponding experimental data will be available.

B. Results for ATLAS cuts

In this subsection we present results relevant for the ATLAS experimental cuts. The following kinematical conditions are imposed:

$$|t_1|, |t_2| < 1\,{\rm GeV}^2, \quad |y_\pi| < 2.5, \quad p_{t,\pi} > 0.5\,{\rm GeV}. \tag{3.2}$$

In addition, the above-mentioned technical cut $M_{4\pi} < 30$ GeV is imposed.

TABLE II. Integrated cross sections in nb with the ATLAS cuts (3.2) for different values of the cutoff parameter $\Lambda_{{\rm off},E}$. No absorption effects are included here.

	$\Lambda_{{\rm off},E}$ (GeV)	σ (nb)
ATLAS	1.0	6.91
ATLAS	1.5	141.43

The corresponding integrated cross sections for different values of the cutoff parameter are collected in Table II. In this case the dependence on $\Lambda_{{\rm off},E}$ is even stronger than for the full phase space case. This means that precise prediction of the cross section is not simple. Similar to the full phase space case, we present several differential distributions in Figs. 10, 11, 12 and 13.

The transverse momentum distribution of the four-pion system is shown in Fig. 10. The shape of the distribution is practically the same as for the full phase space case. It should be noted that the distribution of the longitudinal momentum of the four-pion system after rapidity cuts related to the ATLAS central tracker acceptance (right side of Fig. 21) is very narrow in comparison to full phase space histogram shown in the same figure on the left side. The four-pion invariant mass distribution extends from $M_{4\pi} \approx 3$ GeV to the upper cut at $M_{4\pi} = 30$ GeV. This means that the ATLAS experiment has a potential to investigate the mechanism discussed here.

The rapidity distributions of pions (middle bump) and protons (external peaks) are shown in Fig. 12. Here the rapidity coverage of the main tracker is clearly visible. The rapidity gaps between protons with $y \approx \pm 9$ and pions are now set by the experimental cuts and are bigger than 4.5 rapidity units. However, we have to ensure, in addition, the existence of a rapidity gap within the four-pion system

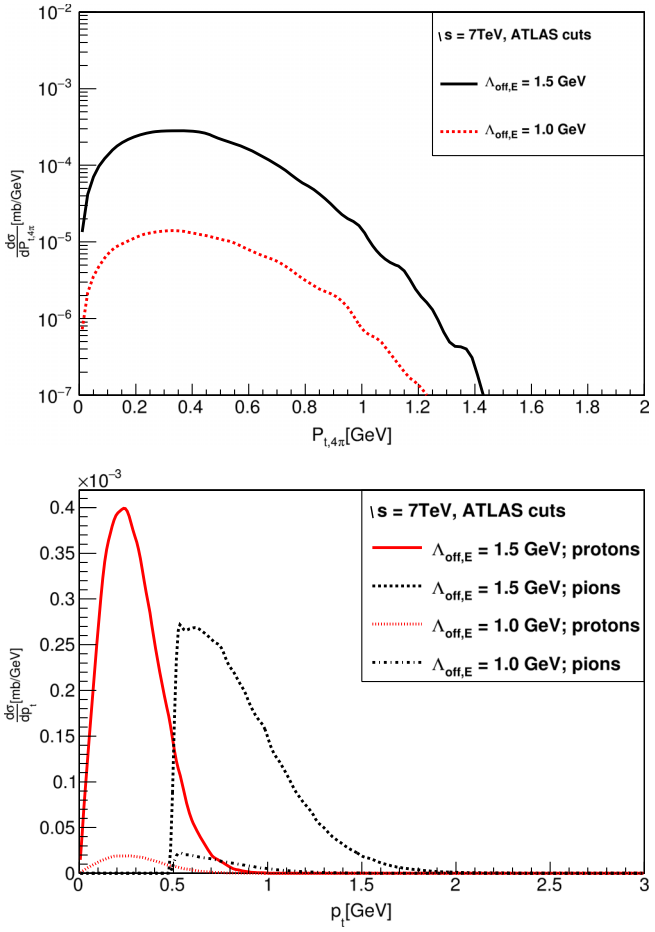

FIG. 10. Distributions in transverse momentum of the four-pion system and for the transverse momenta of individual particles (protons or pions) with the ATLAS cuts (3.2).

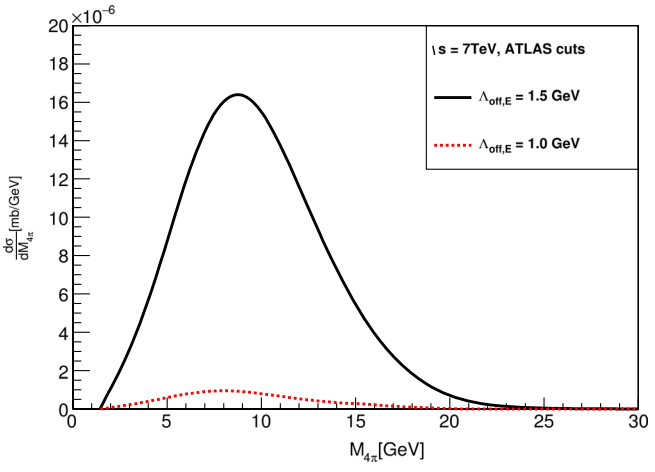

FIG. 11. Four-pion invariant mass distribution ($M_{4\pi}$) with the ATLAS cuts (3.2) for $\Lambda_{\mathrm{off},E} = 1$ GeV (lower curve) and $\Lambda_{\mathrm{off},E} = 1.5$ GeV (upper curve).

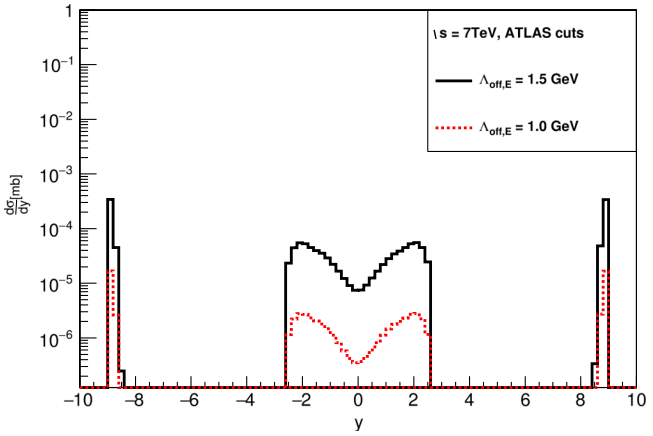

FIG. 12. Distribution in rapidity of pions and protons for the ATLAS cuts (3.2).

confined now to $|y_\pi| < 2.5$. Then the maximal rapidity gap is clearly confined from above to only five rapidity units.

In Fig. 13 we show the dipion invariant mass distribution for the opposite-sign (left panel) and the same-sign (right panel) pions for two different values of $\Lambda_{\mathrm{off},E}$.

One major weakness of the discussed model is a rather simplistic treatment of the low dipion and πp invariant masses, i.e. the non-Regge region. These region can be removed from the data imposing the additional cut $M_{ij} > M_{ij,\mathrm{cut}} \approx 2$–$4$ GeV. Imposing such cuts leads to the cross sections collected in Table III. The rate of the reduction of cross section depends on the value of the cutoff parameter and the way that amplitudes are modified in the difficult-to-control non-Regge region.

These experimental cuts remove influence of the details of the cutoff function on $M_{\pi\pi}$ plots, see Fig. 14. These additional cuts ($M_{ij,\mathrm{cut}} = 2$ GeV) practically do not change the distributions shown in Fig. 13. The same can be seen by comparison of the first two rows of Table III.

C. Results for ALICE cuts

For the ALICE experiment we take the following cuts:

$$p_{t,p} < 2\,\mathrm{GeV}, \quad p_{t,\pi} > 0.17\,\mathrm{GeV}, \quad |\eta_\pi| < 0.9, \qquad (3.3)$$

and the technical $M_{4\pi} < 30$ GeV cut. Corresponding numerical values for the integrated cross sections are presented in Table IV. They are rather small compared to the ATLAS case.

Several differential distributions are presented below in Figs. 16, 17 and 18. The distribution in transverse momentum of the four-pion system (Fig. 15) is here very similar as those for the full phase space and for the ATLAS cuts. In contrast, the distribution in four-pion invariant mass drops faster than its counterpart for the ATLAS case. The irregular structures are due to the narrow rapidity coverage of the ALICE detector and/or the cuts on each exchange of the Pomeron or Reggeon. The cross section for the triple

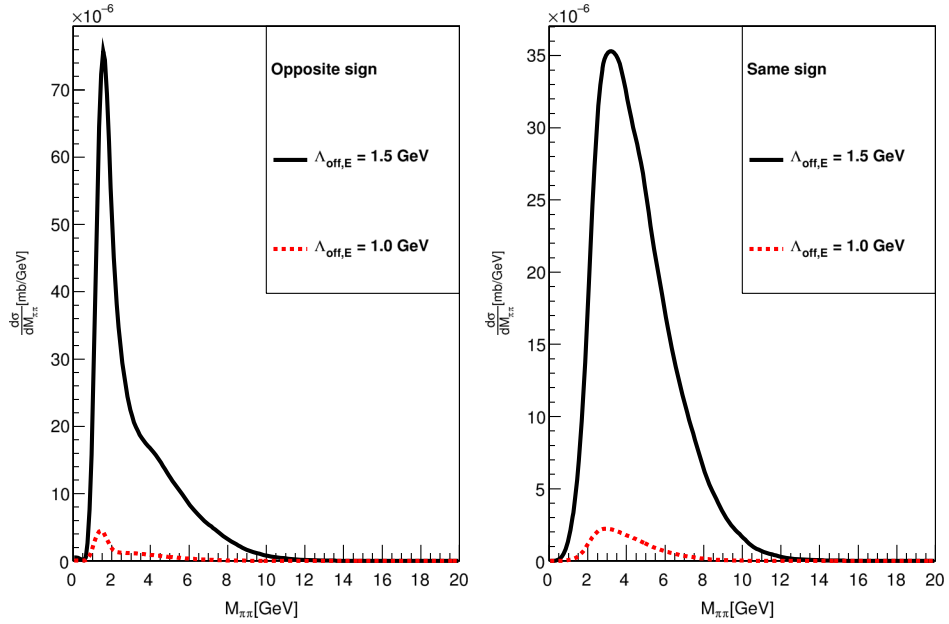

FIG. 13. Dipion invariant mass distribution for the opposite-sign (left) and same-sign (right) pions with the ATLAS cuts (3.2) for different values of $\Lambda_{\mathrm{off},E}$.

Regge mechanism is very small for the ALICE fiducial volume, see Table IV. In addition, other mechanisms (see [8]) may be important in this region. We conclude that the ALICE detector is not well suited for the studies of processes with three Pomeron/Reggeon exchanges.

IV. DISCUSSION OF SOME ADDITIONAL ASPECTS OF THE TRIPLE REGGE EXCHANGE MODEL

Here we discuss in more detail some aspects of the model only mentioned in the previous section.

A. $M_{4\pi}$ distribution and energy transfer to the 4π system

Here we wish to discuss some kinematic properties of the 4π system. In particular, we wish to understand how much energy can be transferred to the four-pion system. In our opinion, this is determined by the fact that the scattered protons take almost all energy, leaving only a small amount of available energy which is distributed among the all centrally produced final pions. This can be traced back to specific propagators of Pomerons/Reggeons that couple to protons. In this subsection we shall try to justify this hypothetical statement.

TABLE III. The integrated cross sections in nb for the ATLAS cuts (3.2) with the extra limitations on $\pi\pi$ and $p\pi$ invariant masses. The "Smooth" columns show the resulting cross sections for the cutoff function of (2.19). The "Sharp" columns show results obtained for the cutoff function of (2.20) with $W_{\mathrm{cut}} = 2$ GeV. No absorption effects are included here.

	$\Lambda_{\mathrm{off},E} = 1.0$ GeV		$\Lambda_{\mathrm{off},E} = 1.5$ GeV	
	Smooth	Sharp	Smooth	Sharp
No extra cut on M_{ij}	7.35	6.91	148.83	141.43
$M_{ij,\mathrm{cut}} = 2$ GeV	7.35	6.90	146.92	141.33
$M_{ij,\mathrm{cut}} = 3$ GeV	6.66	6.31	138.79	134.10
$M_{ij,\mathrm{cut}} = 4$ GeV	5.15	4.82	116.54	113.73

In order to better understand this effect we first plot the distribution in energy of one of outgoing protons in Fig. 19. The distribution quickly drops towards energies smaller than $\sqrt{s}/2$, which in our example is 3.5 TeV. For the case of the ATLAS cuts (3.2) the drop is much faster.

Summing energies of both outgoing protons we obtain total energy taken by protons. In Fig. 20 we show the distribution in the energy left for pions, which is the total energy minus the energy taken away by protons. The energies left for pions are much smaller than those taken away by protons. Kinematics dictates the following inequality:

$$M_{4\pi} < \sqrt{s} - E_1 - E_2. \tag{4.1}$$

For our process the dynamics imposes much more severe cuts, which means the restriction (4.1) is not really important.

In general, the whole four-pion system does not need to be at rest in the overall center-of-mass system. Let us define the quantity

$$P_{4\pi,z} = p_{3,z} + p_{4,z} + p_{5,z} + p_{6,z}. \tag{4.2}$$

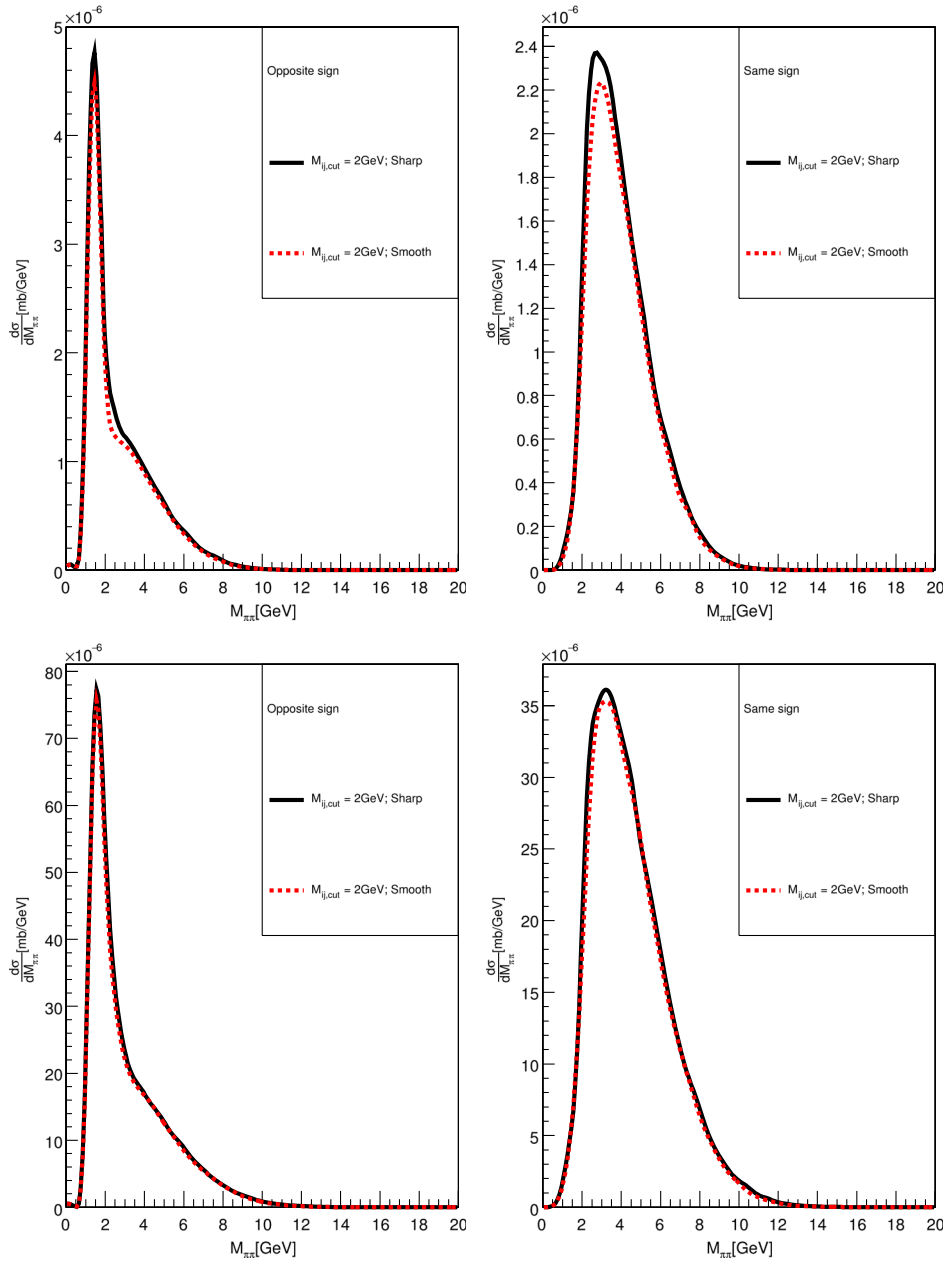

FIG. 14. Dipion invariant mass distributions for the opposite-sign (left) and the same-sign (right) pions for the ATLAS experimental cuts (3.2) with the extra limitations on $M_{ij} > M_{ij,\mathrm{cut}}$. The upper plots are for $\Lambda_{\mathrm{off},E} = 1$ GeV and the lower ones for $\Lambda_{\mathrm{off},E} = 1.5$ GeV. "Smooth" means the cutoff (2.19) with $W_0 = 2$ GeV and "Sharp" means the cutoff (2.20) with $W_{\mathrm{cut}} = 2$ GeV.

TABLE IV. Integrated cross sections in pb for the ALICE cuts (3.3) for the smooth cutoff function and for different values of $\Lambda_{\mathrm{off},E}$. No absorption effects are included here.

	$\Lambda_{\mathrm{off},E}$ (GeV)	σ (pb)
ALICE	1.0	4.2
ALICE	1.5	37.7

In Fig. 21 we show the distribution of the $P_{4\pi,z}$ variable. We observe a much narrower distribution in the case of the ATLAS fiducial volume compared to the full phase space case. In the case of full phase space (upper plot) the four-pion system is created with relatively large longitudinal momenta. For the ATLAS cuts (lower plot) the four-pion system is almost at rest and the whole available energy is transferred to the excitation of the four-pion system.

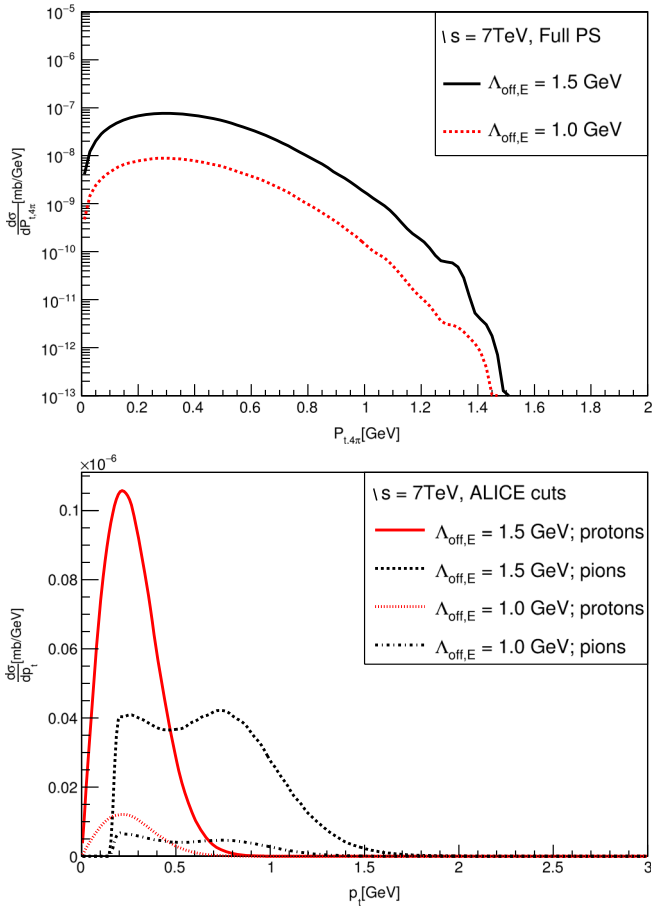

FIG. 15. Distributions in transverse momentum of the 4π system and in transverse momenta of individual pions or protons for the ALICE cuts (3.3) and for the two values of $\Lambda_{\mathrm{off},E}$ specified in the figure legends.

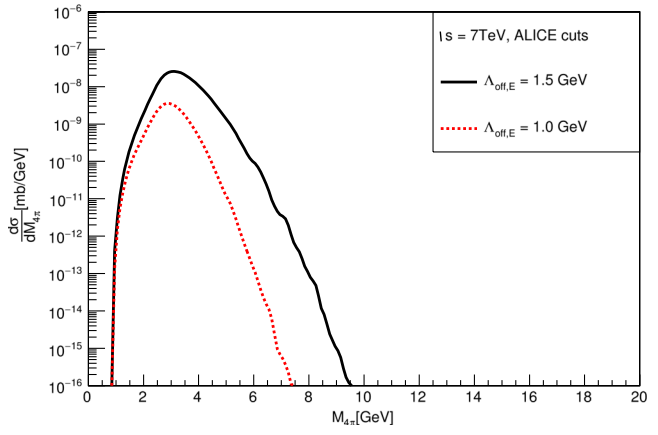

FIG. 16. Four-pion invariant mass distribution for the ALICE cuts (3.3) and for $\Lambda_{\mathrm{off},E} = 1$ GeV (lower curve) and $\Lambda_{\mathrm{off},E} = 1.5$ GeV (upper curve).

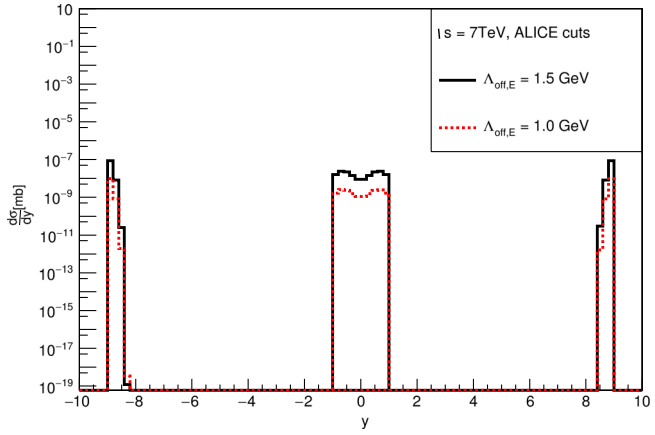

FIG. 17. Distribution in rapidity of pions (middle bump) and of protons (external peaks) for the ALICE cuts for two different values of $\Lambda_{\mathrm{off},E}$.

B. Interference effect

In this subsection we investigate interference between graphs in the whole amplitude. In order to quantify this effect we propose to compare the cross section for the full amplitude of (2.1), with the cross section obtained by adding matrix element squared of individual diagrams, i.e.,

$$|\mathcal{M}_{\text{no interference}}|^2 = \frac{1}{4}(|\mathcal{M}_{\{3456\}}|^2 + |\mathcal{M}_{\{5436\}}|^2 + |\mathcal{M}_{\{3654\}}|^2 + |\mathcal{M}_{\{5634\}}|^2) + \ldots. \tag{4.3}$$

The plots for the full phase space are presented in Fig. 22. The amount of the interference can be considered as a measure of rapidity ordering characteristic for high-energy multiperipheral processes. For fully ordered events, i.e. with large rapidity gaps between all particles, the interference effect is small because identical particles occupy different regions of phase space and the amplitude with reversed order is damped by the factor responsible for the peripherality of the process. In our case the identical pions are often spaced by the large rapidity gap (see Figs. 23 and 24), however, the low rapidity gap spacing component is also strong. As a result, the interference effect contributes to $\sim 1/2$ of the cross section as seen in Fig. 22.

C. Rapidity ordering of pions and the gap between two-pion systems

In this subsection the rapidity gap between different orderings in the rapidity of pions will be presented. This variable can well distinguish different central particles, however, any other variable that separates pions can be used. The procedure can be used in experiment to characterize the triple Pomeron/Reggeon exchange process. The idea is as follows. The pions will be ordered with respect to their rapidities. Assume that the rapidities of

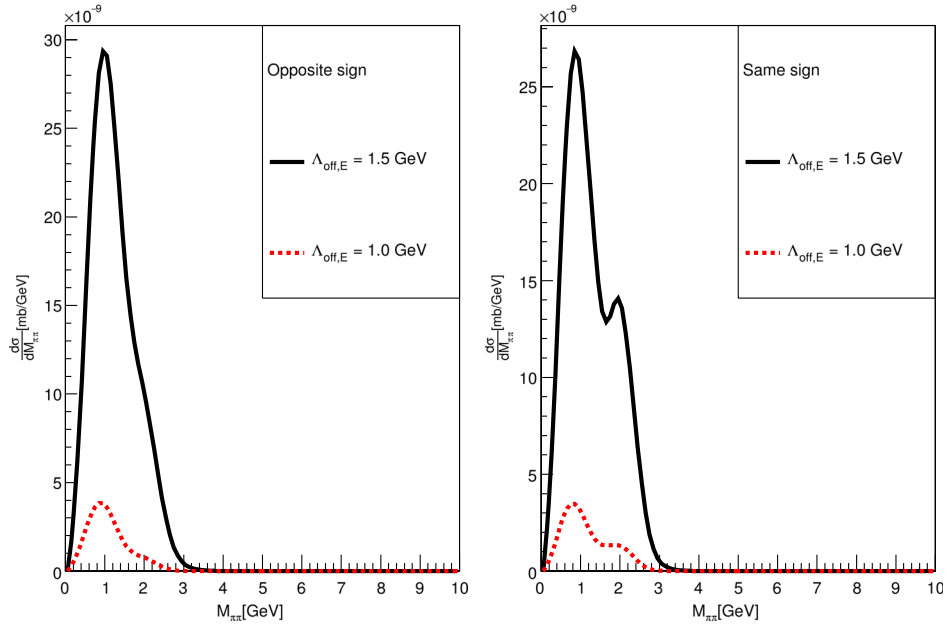

FIG. 18. Dipion invariant mass distribution for the opposite-sign (left) and the same-sign (right) pions for the ALICE cuts (3.3).

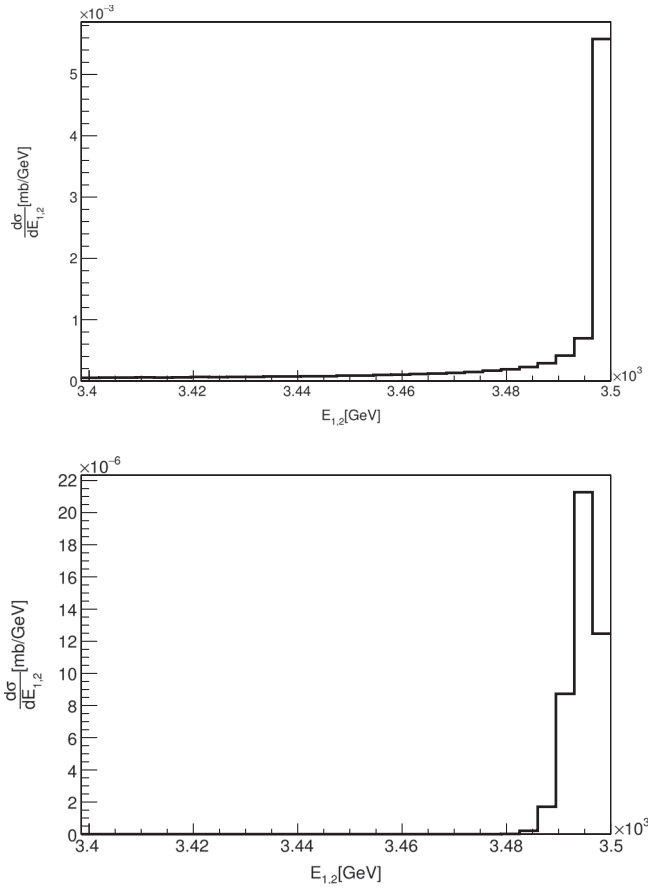

FIG. 19. Proton energy distributions for the full phase space (upper plot) and for the ATLAS cuts (3.2) (lower plot). Here we take $\Lambda_{\mathrm{off},E} = 1.5$ GeV as an example.

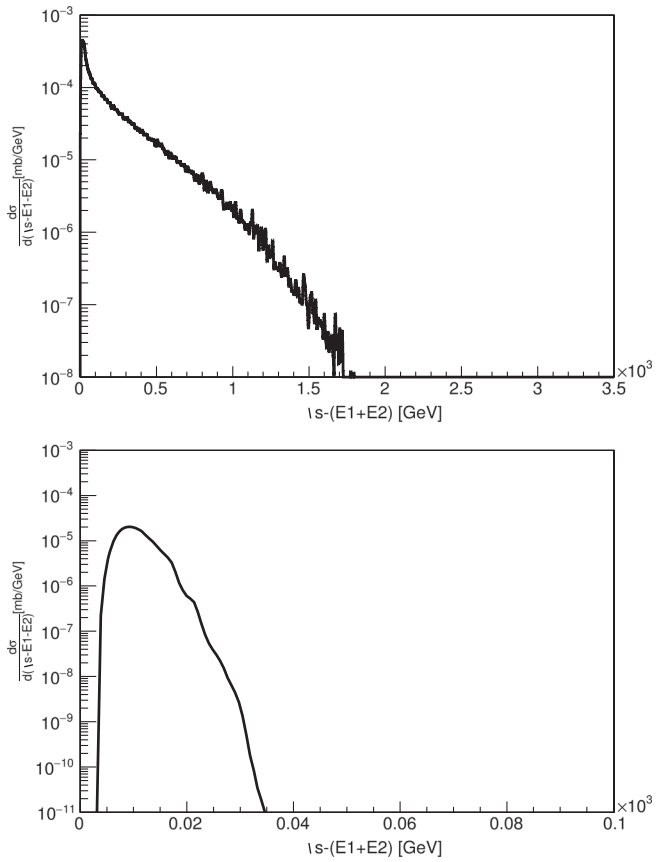

FIG. 20. Distributions in the energy left for pions for the full phase space (upper plot) and for the ATLAS cuts (3.2) (lower plot). Here we take $\Lambda_{\mathrm{off},E} = 1.5$ GeV. For the full phase space case a sharp break above 1500 GeV is visible, indicating a numerical accuracy limit.

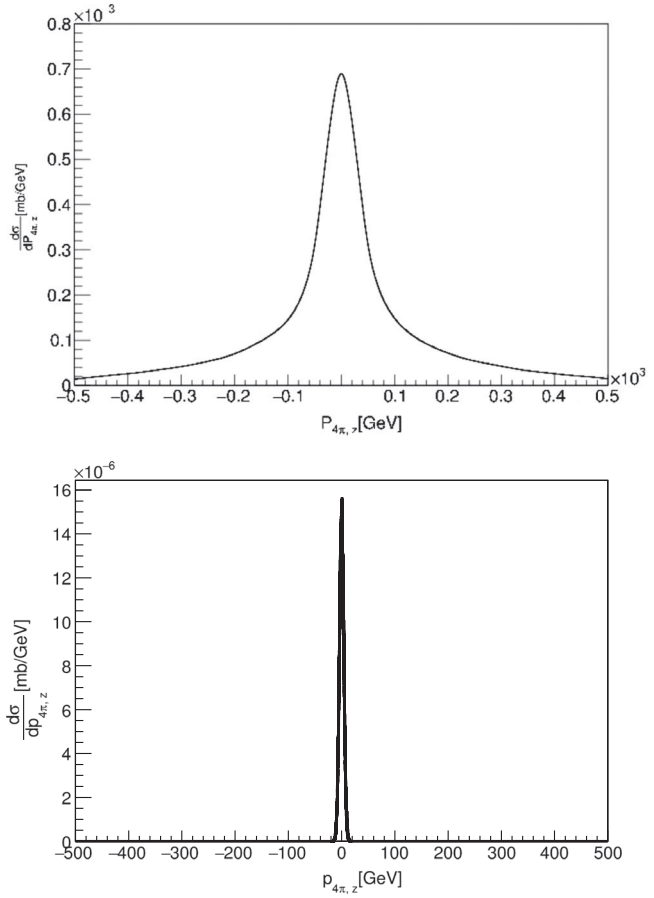

FIG. 21. Distributions in the longitudinal momentum of the pion center of mass for the full phase space (upper plot) and for the ATLAS cuts (3.2) (lower plot). Here we take $\Lambda_{\mathrm{off},E} = 1.5$ GeV as an example.

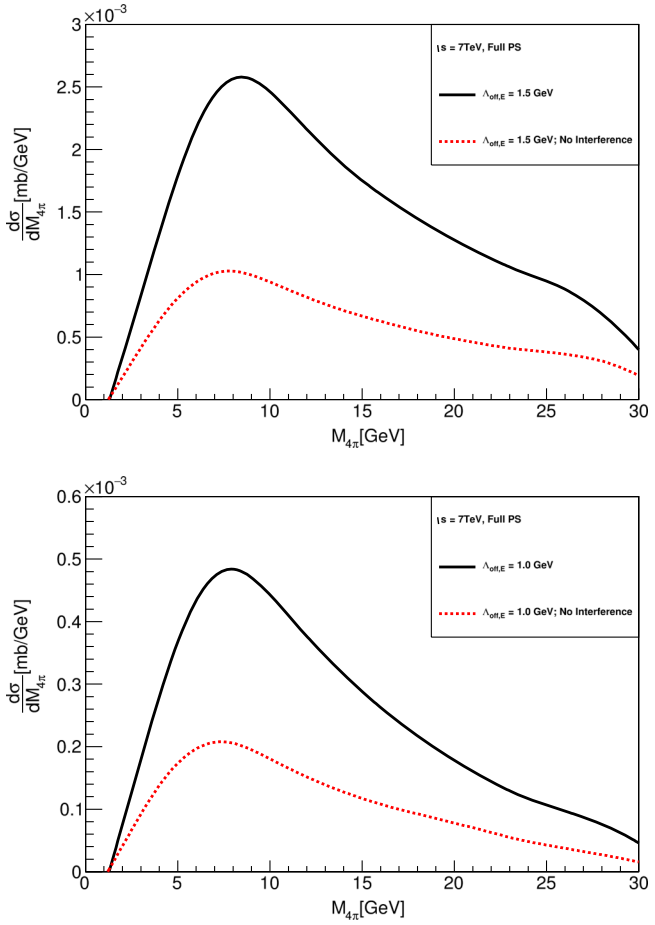

FIG. 22. Four-pion invariant mass distribution for the full phase space for two different values of $\Lambda_{\mathrm{off},E}$.

pions are ordered in the following way: $y_1 < y_2 < y_3 < y_4$. The distribution in rapidity difference between pions 2 and 3 will be presented. Three different classes of the ordering of pion charges are possible in general; specifically, the class A,

(i) $\pi^+(y_1)$, $\pi^-(y_2)$, $\pi^+(y_3)$, $\pi^-(y_4)$,
(ii) $\pi^-(y_1)$, $\pi^+(y_2)$, $\pi^-(y_3)$, $\pi^+(y_4)$,

the class B,

(i) $\pi^-(y_1)$, $\pi^+(y_2)$, $\pi^+(y_3)$, $\pi^-(y_4)$,
(ii) $\pi^+(y_1)$, $\pi^-(y_2)$, $\pi^-(y_3)$, $\pi^+(y_4)$,

and the class C,

(i) $\pi^+(y_1)$, $\pi^+(y_2)$, $\pi^-(y_3)$, $\pi^-(y_4)$,
(ii) $\pi^-(y_1)$, $\pi^-(y_2)$, $\pi^+(y_3)$, $\pi^+(y_4)$.

In Figs. 23 and 24 we present distributions in rapidity difference between the second and the third pion for the full phase space and for the ATLAS kinematical cuts (3.2). These plots show the characteristics of the triple Regge process which can be verified experimentally. As can be seen from the figures, the events for class C happens much more rarely than the events for classes A or B. In addition, the gap for class C is much smaller than for classes A and B. This is because pion exchange is responsible for the gap for the class C versus Pomeron exchange for classes A and B.

D. Comparison with 2σ production

The $pp \to pp\sigma\sigma$ process recently discussed in [8], due to the decay $\sigma \to \pi^+\pi^-$, produces the same final state as the triple Regge $pp \to pp4\pi$ process.

The Born-level results for the continuum mechanism including ATLAS cuts (3.2) for $\sqrt{s} = 7$ and 13 TeV, see Table V, should be compared to 750.56 nb and 847.46 nb, respectively, from the sequential $pp \to pp(\sigma\sigma \to 4\pi)$ process discussed in [8] (please note that slightly different cuts were used there). Note that these values of cross sections are smaller than in Table I of [8], where $p_{t,\pi} > 0.1$ GeV was imposed in the calculations. The cross sections for the $\sigma\sigma$ mechanism were obtained with the coupling constants given by (2.12) of [8] and the off-shell t-channel σ meson form factor (2.13) of [8] with $\Lambda_{\mathrm{off},E} = 1.6$ GeV.

These two mechanisms are complementary as can be seen in Fig. 25, as they occupy different range of $M_{4\pi}$.

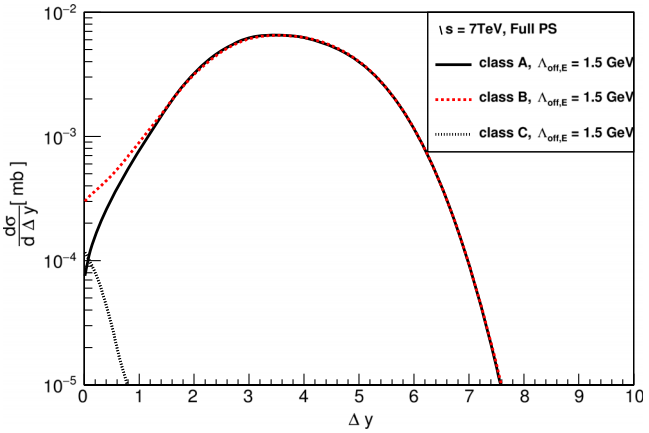

FIG. 23. Rapidity difference between the second and third pion for $\Lambda_{\mathrm{off},E} = 1.5$ GeV for the full phase space.

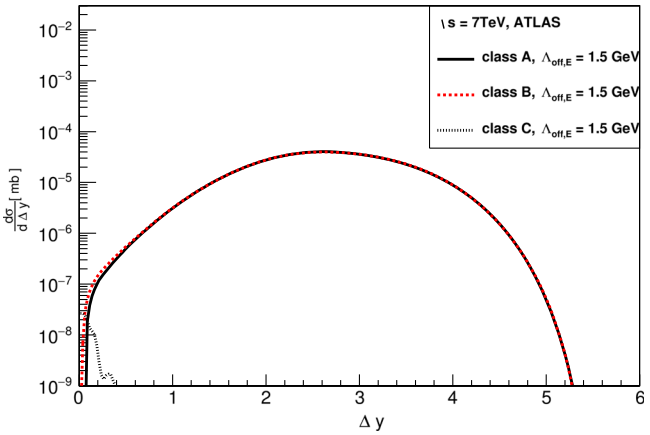

FIG. 24. Rapidity difference between the second and third pion for $\Lambda_{\mathrm{off},E} = 1.5$ GeV for the ATLAS detector cuts.

In addition, in the range 2 GeV $< M_{4\pi} <$ 4 GeV the $\sigma\sigma$ mechanism dominates with a rather sharp peak at $M_{4\pi} \sim$ 3 GeV and the triple Regge contribution dominates above 8 GeV. These characteristics could be very useful when trying experimental distinctions of these two processes.

TABLE V. The integrated Born-level (no absorption effects) cross section for the four-pion continuum production. Results were calculated for two different values of the cutoff parameter $\Lambda_{\mathrm{off},E}$ (2.18).

	$\Lambda_{\mathrm{off},E}$ (GeV)	σ @ $\sqrt{s} = 7$ TeV	σ @ $\sqrt{s} = 13$ TeV
Full PS	1.0	7.21 μb	8.97 μb
Full PS	1.5	42.86 μb	51.78 μb
ATLAS	1.0	6.91 nb	7.48 nb
ATLAS	1.5	141.43 nb	154.19 nb
ALICE	1.0	4.2 pb	4.7 pb
ALICE	1.5	37.7 pb	42 pb

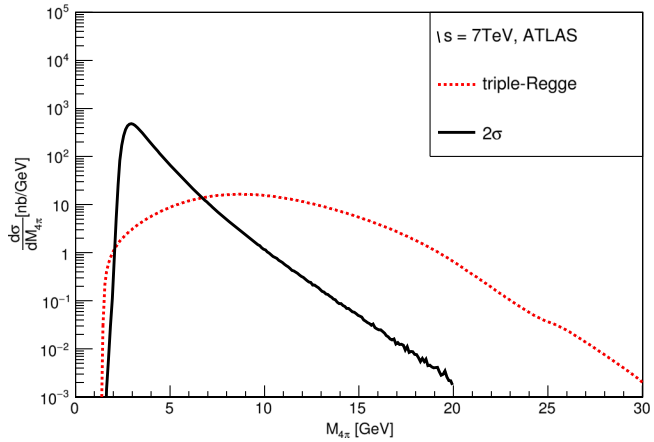

FIG. 25. Four-pion invariant mass distribution ($M_{4\pi}$) with the ATLAS kinematical cuts (3.2) for $\sqrt{s} = 7$ TeV. The results correspond to the Born-level calculations. The dotted line represents the triple Regge exchange mechanism obtained for $\Lambda_{\mathrm{off},E} = 1.5$ GeV. The solid line represents the contribution from $\sigma\sigma$ mechanism discussed in [8].

E. Predictions for LHC at 13 TeV

In this subsection we wish to provide the first predictions for current runs at the LHC at $\sqrt{s} = 13$ TeV. A more detailed analysis, including technical details of experiments, will be postponed to a separate paper.

In Table V numerical values of the cross section are given and compared to our previous results. The table shows that the transfer of energy to the system is slowly varying with the collision energy. Therefore all plots presented in the previous sections do not differ dramatically for the case of $\sqrt{s} = 13$ TeV. The only sizable difference is that in the rapidity plots the protons are a bit further from $y = 0$. Summing up, the model cross section is only weakly dependent on the center-of-mass energy.

V. CONCLUSIONS

The triple Regge exchange model was proposed for the production of four-pions in the $pp \to pp\pi^+\pi^-\pi^+\pi^-$ exclusive reaction. The amplitudes of the process were parametrized in the Regge formalism with coupling constants fixed to describe the total nucleon-nucleon and pion-nucleon cross sections. Some care must be taken how to "remove" the low dipion invariant mass regions ($M_{\pi\pi} < 2$ GeV) that are not described by Regge amplitudes.

In the considered process two of the pions are off-mass-shell already in the Born amplitude(s). The off-shell effects are parametrized in terms of corresponding form factors. The same objects (form factors) were discussed recently in the context of the $pp \to pp\pi^+\pi^-$ reaction considered both theoretically as well as measured by the STAR, CDF and CMS collaborations [11–13]. The cutoff parameter was fitted then [6] to describe the preliminary data. The present

dipion data do not allow for a precise extraction of the model parameter but do allow us to obtain a reasonable range of the cutoff parameter $\Lambda_{\mathrm{off},E} = 1$–$1.5$ GeV. Here we have assumed exponential dependence of the form factors on the pion virtualities. Then the model has almost only one free parameter (called here the cutoff parameter), which can be taken in the range known from the four-body ($pp \to pp\pi^+\pi^-$) reaction studied in the literature. In comparison to the four-body reaction the dependence on the cutoff parameter is much stronger because two pions, instead of one for the $pp \to pp\pi^+\pi^-$ process, are off-mass-shell.

We have made first predictions for the six-body processes. Both total cross sections (integrated over the six-body phase space) as well as several differential distributions were calculated and presented. Compared to the $\sigma\sigma$ and $\rho\rho$ mechanisms considered recently by two of us [8], the mechanism considered here populates final states with much larger dipion and four-pion invariant masses. We get total cross section $7.21 - 42.86$ μb (see Table V) in the whole phase space (neglecting absorption effects!). The absorption effects are expected to diminish the cross section by an order of magnitude. Our preliminary studies here have been done at the Born level and the absorption can be included only in the form of the multiplicative gap survival factor. One expects it to be of the order of 0.1. The full-fledged calculation of absorption effects, and in particular its dependence on kinematical variables, is not simple (see e.g. [14] for detailed studies for the $pp \to pp\pi^+\pi^-$ reaction).

The integrated full phase space cross section, however, cannot be measured due to limited coverage of the LHC detectors. We have therefore made predictions for the kinematical cuts characteristic for the ATLAS and ALICE detectors. The latter detector can identify pions down to very small transverse momenta of $p_{t,\pi} = 0.1$ GeV. However, the rapidity coverage of the ALICE tracker is very (too) limited. This does not allow us to observe the large four-pion invariant masses, the genuine feature of the considered diffractive triple Regge mechanism. In contrast, the ATLAS detector allows us to measure cases with large 4π invariant masses. We expect that the considered multidiffractive process dominates over the contributions of other mechanisms for four-pion invariant masses $M_{4\pi} > 10$ GeV.

We have discussed, in addition, how much energy can be transferred from protons to the excitation of the four-pion system. We have demonstrated that the model amplitude gives natural limitations for such a transfer. A specific ordering of pion charges in rapidity has been found to be an interesting and representative characteristic of the discussed process.

To ensure exclusivity of the process, not only charged pions but also forward/backward protons should be measured. The ALFA detectors are natural candidates for this purpose in the case of the ATLAS experiments. Similarly, the CMS Collaboration together with the TOTEM Collaboration could perform similar studies.

In summary, the observation of counts/events at large four-pion invariant masses should be a clear signal of observing the three-Pomeron exchange processes discussed here, which have not been identified so far experimentally.

In the present studies we have considered only the four-pion continuum. In principle, the Pomeron-Pomeron fusion may lead to a production of mesonic resonances (see e.g. [15,16]). Then, intermediate states with mesonic resonances, such as $\pi^+\pi^-(R \to \pi^+\pi^-)$ or $R_1(\to \pi^+\pi^-)R_2(\to \pi^+\pi^-)$, also have to be considered, and then $\sigma, f_0(980), f_2(1270), f_0(1500)$ and others have to be included. In order to remove such resonances one can impose lower cuts on all combinations of $\pi^+\pi^-$ invariant masses.

If the measurement is not able to guarantee full exclusivity (no measurement of forward protons) then excitations of one or both protons have to be considered in addition. Some works on this subject have been started only recently [17,18]. We expect that such processes could lead to increase of the cross section by 20%–40%.

ACKNOWLEDGMENTS

This work was supported in part by the Polish National Science Centre Grant No. 2014/15/B/ST2/02528, the Ministry of Science and Higher Education Republic of Poland Grant No. IP2014 025173 (Iuventus Plus) and by the Center for Innovation and Transfer of Natural Sciences and Engineering Knowledge in Rzeszów. This research was supported in part by PLGrid Infrastructure. Some calculations were also supported by Cracow Cloud One infrastructure.

APPENDIX: PERIPHERAL REACTION WITH THE DECAY OF THE CENTRAL SYSTEM

In this appendix we present the recipe for generating phase space of the reaction which treats all final pions in the same way and therefore it is suitable for the case when including complicated interferences of contributing amplitudes. The considered reaction is of the form $p(p_a) + p(p_b) \to p(p_1) + p(p_2) + CM(P_{4\pi})$, and then $CM(P_{4\pi}) \to \pi^+(p_3) + \pi^-(p_4) + \pi^+(p_5) + \pi^-(p_6)$. The formula for the cross section can be written in the standard form,

$$\sigma = \int (2\pi)^4 \frac{\overline{|\mathcal{M}|^2}}{2s} \delta^{(4)}\left(P - \sum_{i=1}^{6} p_i\right) \prod_{i=1}^{6} \frac{d^3 p_i}{(2\pi)^3 2E_i}, \quad \text{(A1)}$$

where $\mathcal{M}$ is a matrix element for the six-body reaction and $P = p_a + p_b$ is a total four-momentum in the initial (and final) system.

Starting from (A1) the phase space is factorized as [see [19], Eq. (9.7)]

$$\sigma = \int_{4m_\pi}^{\infty} dM_{4\pi}^2 \int (2\pi)^4 \delta^{(4)}(P - p_1 - p_2 - P_{4\pi}) \times \frac{d^3p_1}{(2\pi)^3 2E_1} \frac{d^3p_2}{(2\pi)^3 2E_2} \frac{d^3P_{4\pi}}{(2\pi)^3 2E_{4\pi}} \times \frac{1}{2\pi} \int (2\pi)^4 \delta^{(4)}\left(P_{4\pi} - \sum_{i=3}^{6} p_i\right) \prod_{i=3}^{6} \frac{d^3p_i}{(2\pi)^3 2E_i} \frac{\overline{|\mathcal{M}|^2}}{2s}, \tag{A2}$$

where the integration over the $M_{4\pi}$ variable extends from the threshold for the 4π production to the infinity (in our case to the technical cut $M_{4\pi} < 30$ GeV). The second decay of the central system $P_{4\pi}$ into four particles can be calculated using a slightly modified sequence of decays of the GENBOD CERN library (currently the TGenPhaseSpace class from ROOT package [20]). For a description of the algorithm of the generation see [21]. This modification will be described elsewhere.

This prescription is the best choice for matrix elements with permutation of identical particles, as it treats all centrally produced particles on the same footing.

In our practical realization the phase space available for the process is fairly large which requires special technical treatment event for adaptive Monte Carlo generator. The most efficient solution is to divide the whole range of $M_{4\pi}$ into smaller exclusive intervals and add distributions for the different intervals.

[1] P. Lebiedowicz and A. Szczurek, Phys. Rev. D **81**, 036003 (2010).
[2] R. Staszewski, P. Lebiedowicz, M. Trzebinski, J. Chwastowski, and A. Szczurek, Acta Phys. Pol. B **42**, 1861 (2011).
[3] P. Lebiedowicz and A. Szczurek, Phys. Rev. D **83**, 076002 (2011).
[4] P. Lebiedowicz and A. Szczurek, Phys. Rev. D **85**, 014026 (2012).
[5] R. A. Kycia, J. Chwastowski, R. Staszewski, and J. Turnau, arXiv:hep-ph/1411.6035.
[6] P. Lebiedowicz, O. Nachtmann, and A. Szczurek, Phys. Rev. D **93**, 054015 (2016).
[7] A. Breakstone *et al.* (ABCDHW Collaboration), Z. Phys. C **58**, 251 (1993).
[8] P. Lebiedowicz, O. Nachtmann, and A. Szczurek, Phys. Rev. D **94**, 034017 (2016).
[9] D. A. Fagundes, L. Jenkovszky, E. Q. Miranda, G. Pancheri, and P. V. R. G. Silva, Int. J. Mod. Phys. A **31**, 1645022 (2016).
[10] A. Donnachie, H. G. Dosch, P. V. Landshoff, and O. Nachtmann, *Pomeron Physics and QCD*, Cambridge Monographs on Particle Physics, Nuclear Physics and Cosmology Vol. 19 (Cambridge University Press, Cambridge, England, 2002).
[11] L. Adamczyk, W. Guryn, and J. Turnau, Int. J. Mod. Phys. A **29**, 1446010 (2014).
[12] T. A. Aaltonen *et al.* (CDF Collaboration), Phys. Rev. D **91**, 091101 (2015).
[13] CMS Collaboration, Report No. CMS-PAS-FSQ-12-004.
[14] P. Lebiedowicz and A. Szczurek, Phys. Rev. D **92**, 054001 (2015).
[15] R. Fiore, L. Jenkovszky, and R. Schicker, Eur. Phys. J. C **76**, 38 (2016).
[16] P. Lebiedowicz, O. Nachtmann, and A. Szczurek, Phys. Rev. D **93**, 054015 (2016).
[17] A. Cisek, W. Schäfer, and A. Szczurek, Phys. Lett. B **769**, 176 (2017).
[18] P. Lebiedowicz, O. Nachtmann, and A. Szczurek, Phys. Rev. D **95**, 034036 (2017).
[19] H. Pilkuhn, *The Interactions of Hadrons* (North-Holland Publishing Company, Amsterdam, 1967).
[20] ROOT software, http://root.cern.ch/drupal/.
[21] F. James, CERN Report No. 68-15, 1968.